CFD lab, Test Case 1
Laminar oil transport in a pipeline

Marta Pignatelli

July 28, 2025

General Information

Report for the first test case of the Computational Fluid Dynamics laboratories within the course of Fluids Labs, by G. V. Messa, Politecnico di Milano.

1 Introduction

The case under observation is the laminar flow of a heavy crude oil in a pipeline. The simulation will be taken using PHOENICS software and data will be post-processed through MATLAB.

2 Case description

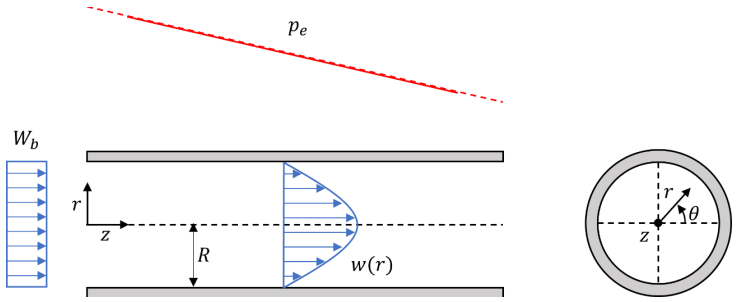

Figure 1: Sketch of the case

A uniform velocity profile is given as inflow, but, if the pipeline is long enough, one expects the flow to reach a fully developed state at a certain distance downstream of the left edge, and this must be reproduced by the CFD solution. The fully developed laminar flow admits an analytical solution, the cylindrical Poiseuille flow:

$$w(r,\theta,z) = w(r) = -\frac{1}{4\mu}\frac{dp_e}{dz}(R^2 - r^2)$$
$$u(r,\theta,z) = 0$$
$$v(r,\theta,z) = 0$$
$$\frac{dp_e}{dz} = const < 0$$
$$\tau_{rz}(r,\theta,z) = -2\mu\frac{1}{2}\left(\frac{\partial v}{\partial z} + \frac{\partial w}{\partial r}\right) = -\mu\frac{dw}{dr} = -\frac{dp_e}{dz}\frac{r}{2}$$

where μ is the dynamic viscosity of the fluid, R is the inner radius of the pipe, u, v, w are the velocity components along the directions θ, r, z (see Figure 1 and Figure 2), p_e is the excess pressure and τ_{rz} is the only non-zero shear stress term.

2.1 Numerical simulation

The steady-state formulation of the Navier-Stokes equations is solved. The problem will be simulated as 2D through a domain having the shape of a circular sector, as shown in Figure 2, and hence it will be realized in PHOENICS by means of cylindrical coordinates.

- **Inlet boundary condition:** a uniform z-velocity profile equal to W_b (bulk velocity) is imposed, whereas the r- and θ- velocity components are set to zero;
- **Outlet boundary condition:** the excess pressure is specified to a null value;
- **Wall condition:** walls are assumed to be fixed and a no-slip condition is set;
- **Axisymmetry condition:** as default in such coordinates' system, it's exploited to reduce the computational burden of the simulations.

This set of boundary conditions results in a developing flow field, which should reach a fully developed state within the computational domain.

2.2 Configuration of the problem

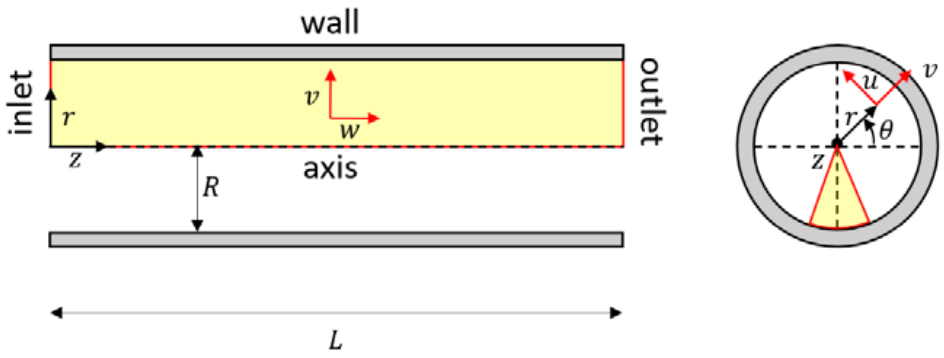

Figure 2: Domain and boundary conditions

Pipe diameter $2R = 150\ mm$,
Bulk velocity $W_b = 0.45\ m/s$,
Fluid = heavy crude oil with:
density $\rho = 910\ kg/m^3$
kinematic viscosity $\mu = 3.5 \times 10^{-4}\ m^2/s$

3 Analysis

3.1 Verify laminarity

To check that the flow is laminar, we can simply compute the Reynolds bulk number Re_b of the problem and verify whether it satisfies the rule $Re_b < 2000$.

$$Re_b = \frac{W_b \cdot D}{\nu} = 192.85 < 2000$$

Indeed, it is below the threshold of turbulent flow.
Furthermore, we could verify the incompressibility of the fluid by computing the Mach number Ma and checking whether it satisfies $Ma < 0,3$. Unfortunately, Ma is defined as the ratio between a characteristic velocity of the problem, which could be W_b, and the velocity of sound in the fluid, which we are not given. We assume the fluid to be incompressible anyway.

Study of domain length

The goal is to define a length that is sufficient to observe a fully developed flow. We recall that such state is characterized by:

$$\frac{\partial \phi}{\partial z} = 0 \quad \forall \phi \neq p_e$$

Moreover, we explicit that it's not our intention to optimize such length, and derive the so called *entry length* L_e, to reduce computational costs, also considering that this type of simulation is not particularly demanding.

For the sake of generality, we start by making use of dimensionless variables; hence we are going to rescale the lengths by dividing them by the radius of the pipe R. We select, for example, a ratio of $k = 30$, thus taking in consideration a length $L = 2.25\ m$.

Then we set up the simulation, choosing a quite refined grid in order to be in the grid-independent region of the solution[1]. In table 1, there are shown the grid parameters: note that the number of cells along the z-axis is proportional to the number of cells in the y direction, with a multiplicative coefficient of k. Additionally, the non-null power law is the option set to get a non-uniform mesh: since the critical region should be near the wall, the refinement is higher there.

	#cells	power law
$x = \theta$	1[2]	none
$y = r$	10	-1.5
z	300	none

Table 1: Specifics of the chosen mesh.

Setting a maximum of 1000 iterations and a global convergence threshold of 10^{-3}, we obtain:

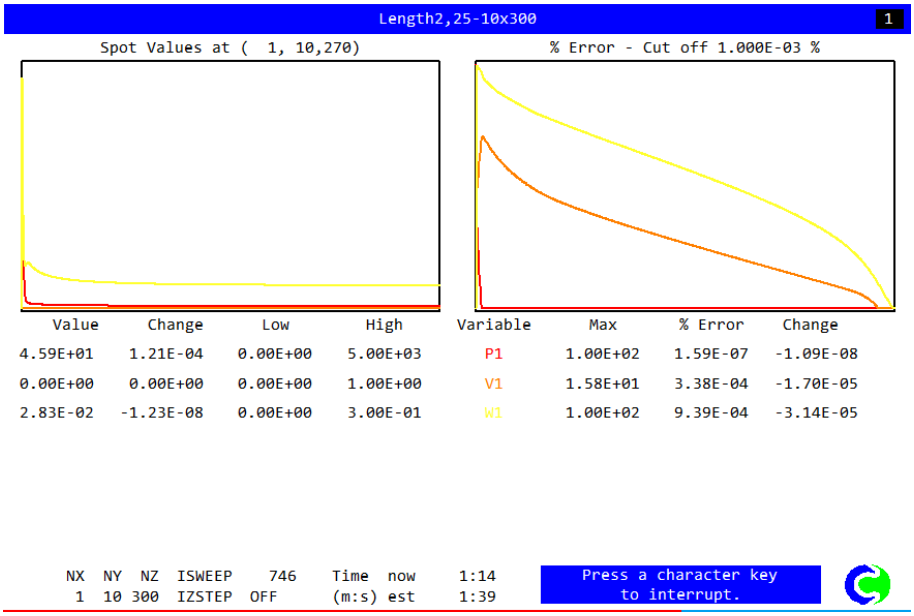

Figure 3: Spot values and residuals

Hence the simulation converges in 746 iterations and the fields look quite stable in the cell near the wall, at about 90% of the length, where the probe is put.

[1] We will see in the paragraph 3.3 whether we can accept these results.

[2] This is intended to obtain a 2D simulation.

We inspect the colour plots of pressure and velocity:

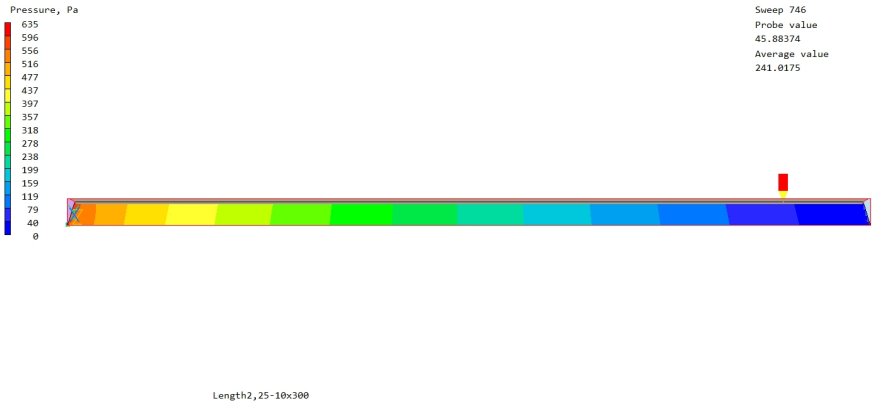

Figure 4: Pressure field

Figure 5: Velocity

Qualitatively, the pressure field seems indeed physically sound: in particular, it seems rather homogeneously descending in the last part of the pipe. The velocity may seem to be invariate from about 65% of the domain onward: that is the portion of tube where we could assume the flow to be fully developed.
To confirm such hypothesis, applying a quantitative criterion is necessary. We decide to look at the values of $\frac{\partial w}{\partial z}$, saved from the PHOENICS environment, along the z-axis, both near the centre of the cylinder, where velocity reaches its maximum value, and near the edge, where velocity patterns should be more interesting. We state that fully developed state is obtained if such derivatives go below the arbitrary threshold of 1% .
We process the data in MATLAB and we get that, starting from exactly 90% of length downstream of the inlet (which corresponds to $k \cdot 0.9 = 27$ times the radius of the pipe), the flow stabilizes (it satisfies our chosen criterion) in each of the cells. See Figure 6.

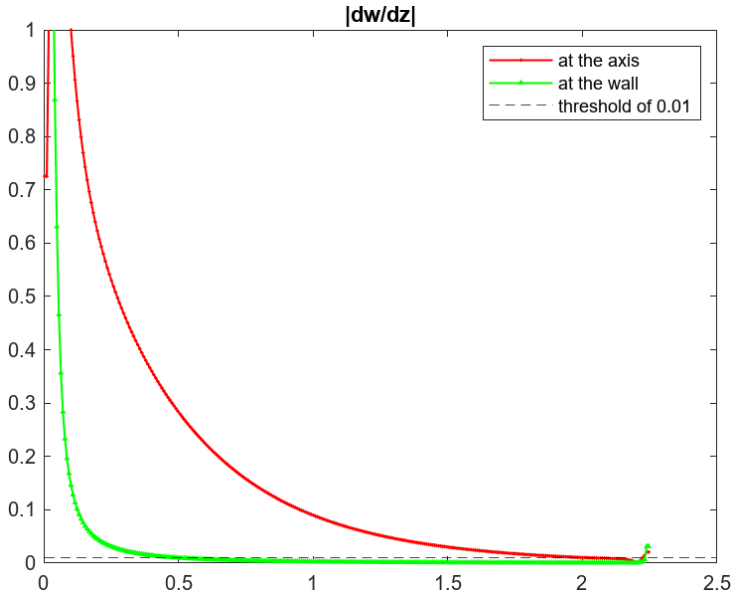

Figure 6: Zoomed plot of $|\frac{\partial w}{\partial z}|$

Entrance lengths L_e found in the literature are various and mostly qualitative; we report just some of them[3]:

- From [2], [3], we see the Hagen-Poiseuille law: $L_{h,laminar} = 0.0575\ Re_D\ D$.
  It's the most common estimate and the value of $0.0575\ Re_D\ D \simeq 22,2\ R$ is lower than the one we provided, so our criterion is a bit more restrictive;

- Nikuradse [4] suggests a quite higher estimate: $L > 40D = 80R$.
  This value would instead invalidate our result. Deepening into the source, it may be due to the fact that this inequality is given for turbulent flow, which is not our case.

- Ahmad and Hassan et al.[5], conducting experiments in rectangular microchannels, came to propose $\frac{L}{D_h} = \frac{0.6}{0.14\ Re\ +\ 1} + 0.0752\ Re \simeq 29\ R$, which would agree with our result.

- Hao et al. [6] found that the correlation between entrance length and the Reynolds number Re was $\frac{L}{D_h} = (0.08 - 0.09)\ Re$, where D_h is the hydraulic diameter and the "-" is intended as range. We read that it's obtained by imposing that the centerline velocity equals 99% of its maximum speed. This provides a value of about $30 \cdot R$, which is similar to our measure.

- In the work of Renksizbulut and Niazmand et al. [7], just like this example, the measurements on which the conclusion takes ground consider a uniform inlet profile (which is reckoned not too reliable by other studies, since it is not a realistic situation). The estimate given is quite complex and it involves heat transfer and geometric parameters, so we will not dwell much on it.

- Galvis and Yarusevych et al. [8] got to the formula $\frac{L}{D_h} = \frac{0.74}{0.09\ Re\ +\ 1} + 0.0889\ Re$ that is appproximately equal to 34 Re, still not too far from our guess.

3.2 Solution inspection

To verify that the solution is physically sound, we inspect the colour plots of pressure and velocity, reported in Figure 4 and 5. Qualitatively, they appear to be fine, showing no weird patterns; the variables behave as one would expect. Another thing to put attention to is the

[3]Many of the following are taken from this article [1].

velocity in the y-direction (r-direction): as it should be, it is (almost) null in most of the domain (see Figure 7 below).

Figure 7: Colour plot of r-velocity

Moreover, we can take a look at the curves of the target quantities along a segment. Regarding the pressure, it is in our interest to show how it evolves along the centerline and near the wall, parallel to the z-axis. In the graph in Figure 8, it is nice to notice that, indeed, the pressure decreases linearly in the (supposed) fully developed region. Additionally, we acknowledge that the pressure gradient is higher at the wall in the beginning (in the developing region) and this matches with the fact that, being the flow pressure-driven, a bigger pressure drop is needed to adapt to the wall condition (no-slip condition).

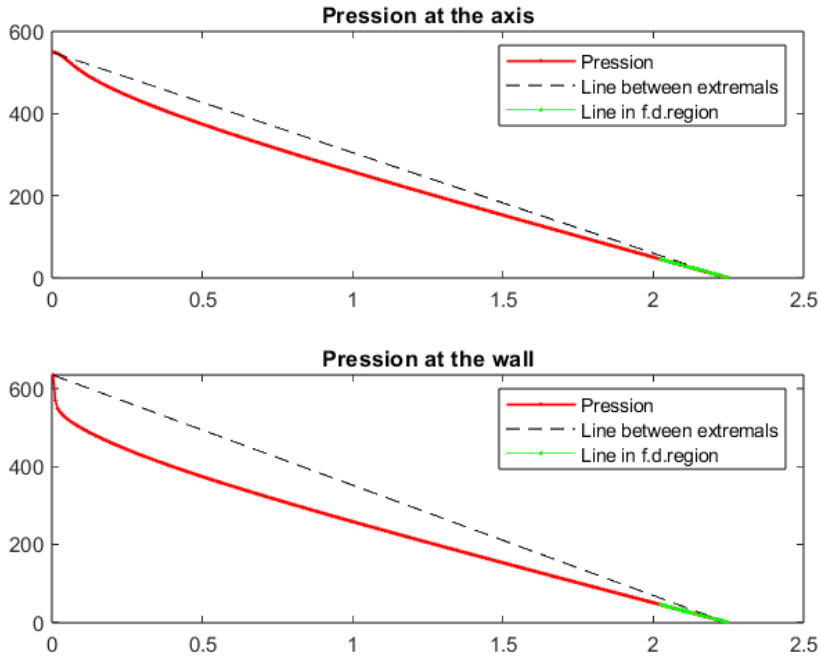

Figure 8: Pressure curves along z-direction

Concerning the velocity, we investigate its profile along the radius at several fixed z positions. In Figure 9a, the produced plot exhibits that the boundary conditions are correctly applied and the trajectory fast tends to a parabolic arch. Finally, we also checkout the centerline velocity and we can appreciate its increase going downstream, ending in a non physical null value, due

to the user-set outlet conditions (see Figure 9b).

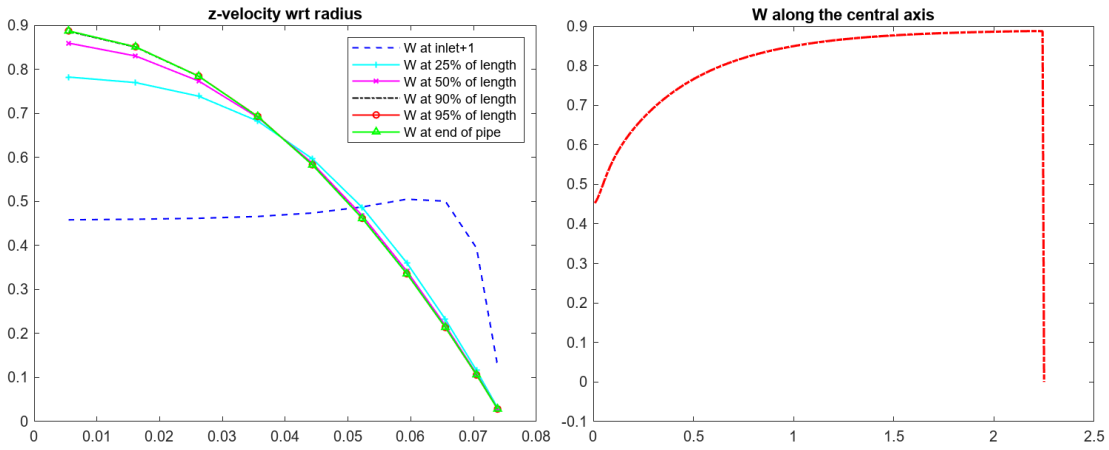

(a) z-velocity at various cross sections of pipe (b) z-velocity at the central axis

Figure 9

3.3 Numerical convergence

- Convergence of simulation
  As one can detect from Figure 3, the simulation achieves convergence in 746 iterations, it does not display oscillations, and the whole-field residuals constantly reduce towards the chosen threshold.

- Grid independence study
  The target parameters of the grid independence study are W, $\frac{\partial W}{\partial y}$ and P. The reference domain is a cylinder with $L = 30R$, as used before. In table 2 are reported the meshes on which the study has been carried out. In each of them, the distribution of the cells is not uniform, but it follows a power law of -1.5 along the radius direction, such that the more critical wall region is resolved in a finer way.
  The method adopted consists of comparing 2 more refined meshes to a reference one. These two are constructed in 3 ways: refining only along the y-direction, only along the z-direction and then both together, maintaining the same aspect ratio of the cells.

ID	# cells	$x = \theta$	$y = r$	z
base	3000	1	10	300
z1	4000	1	10	400
z2	6000	1	10	600
y1	4500	1	15	300
y2	6000	1	20	300
yz1	6750	1	15	450
yz2	12000	1	20	600

Table 2: Parameters of the meshes for the grid independence study

The results are promising: as shown in the following figures, each variable is proven grid independent, since increasing the refinement the relative difference of values decreases (this indicates convergence). It is noticeable that refinements along the z-direction define absolutely negligible variations, non qualitatively visible. On the contrary, modifying the cells' dimensions with respect to the other axis, creates visible changes. That phenomenon is

obviously particularly relevant for $\frac{\partial W}{\partial y}$, but also for the z-velocity near the wall, because the grid permits to get values that approximate better the null wall condition.

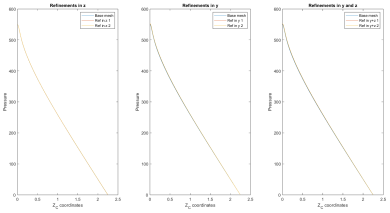

(a) Pressure

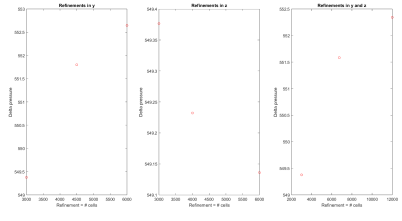

(b) ΔP

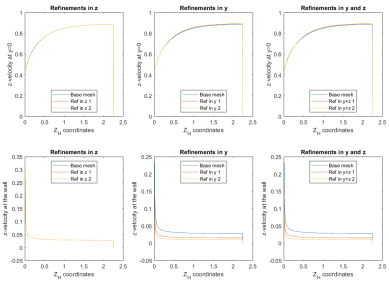

(c) z-velocity

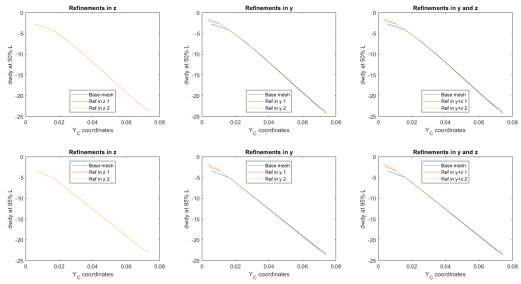

(d) $\frac{\partial W}{\partial y}$

Figure 10: Grid independence plots

3.4 Validation

Since the laminar flow in a cylindrical pipe admits an analytic solution, we perform benchmarking of our results. Being given W_b, we first need to manipulate the equations (2) to make them functions of our datum, instead of $\frac{\partial p}{\partial z}$.

$$
\begin{aligned}
W_b &= \frac{Q}{\pi R^2} = \\
&= \frac{1}{\cancel{\pi} R^2} \int_0^R w(r) \cdot 2\cancel{\pi} r \, dr = \\
&= \frac{1}{\cancel{4}_{\,2}\, \mu R^2} \frac{\partial p}{\partial z} \cancel{2} \int_0^R (R^2 r - r^3)\, dr = \\
&= -\frac{1}{8\mu} \frac{\partial p}{\partial z} R^2 \\
&\Rightarrow \frac{\partial p}{\partial z} = -\frac{8\mu}{R^2} W_b
\end{aligned}
$$

Hence, our system becomes:

$$
\begin{aligned}
w(r) &= -\frac{1}{4\mu} \cdot (-\frac{8\mu}{R^2})(R^2 - r^2)\ W_b = 2\ \frac{R^2 - r^2}{R^2}\ W_b \\
\tau_{rz}(r, \theta, z) &= -\frac{\partial p}{\partial z} \frac{r}{2} = 4\mu \frac{r}{R^2}\ W_b
\end{aligned}
$$

To compare the theoretical shear stress with its simulated counterpart, we compute an approximation of $\frac{\partial p}{\partial z}$ by taking two points at 90% and 95% of the length and dividing their difference by their distance. In the fully developed region, the L_∞errors we get for $w = z$-velocity and τ_{rz}

are respectively 0.0088 and 0.0024.

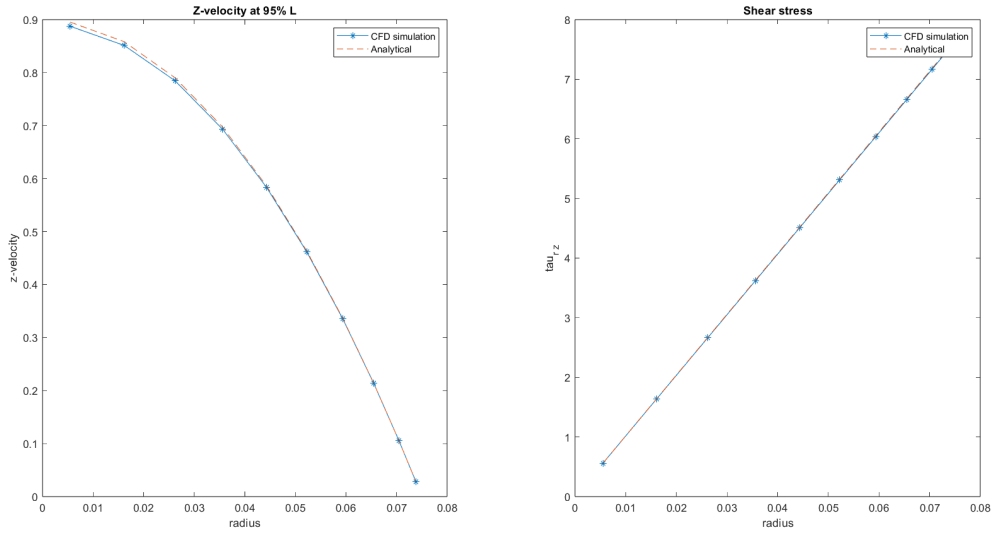

Figure 11: Benchmarking plots

3.5 Friction factor trend

To obtain the trend of the friction factor f versus the bulk Reynolds number, Re_b, we manipulate the analytical solution.

$$f = \frac{8\tau_w}{\rho W_b^2}$$
$$\tau_w = \tau_{rz}|_{r=R} = \frac{4\mu}{R} W_b$$
$$\Rightarrow f = \frac{32\mu}{\rho W_b R} = \frac{64}{Re_b}$$

To compare the analytical friction factor with the approximated one, we compute the latter by means of the simulated pressure (see eq. (3.5)) and we get a relative error of 0.0024.

$$f_{CFD} = -\frac{2D}{\rho W_b^2}\frac{\Delta P}{\Delta z}$$

References

[1] Haiwang Li, Yujia Li, Readmore Huang, and Tiantong Xu. Flow characteristics of the entrance region with roughness effect within rectangular microchannels. *Micromachines*, 11:30, 12 2019.

[2] T. L. Bergman and Frank P. Incropera. *Fundamentals of heat and mass transfer*. Wiley, Hoboken, NJ, 7 edition, 2011.

[3] F. M. White. *Fluid Mechanics*. McGraw- Hill, 7 edition, 2011.

[4] Johann Nikuradse. *Gesetzmässigkeiten der turbulenten Strömung in glatten Rohren: aus d. Kaiser-Wilhelm- Institut für Strömungsforschg, Göttingen*. VDI-Verlag, 1932.

[5] Tariq Ahmad and Ibrahim Hassan. Experimental analysis of microchannel entrance length characteristics using microparticle image velocimetry. 2010.

[6] Peng-Fei Hao, Feng He, and Ke-Qin Zhu. Flow characteristics in a trapezoidal silicon microchannel. *Journal of Micromechanics and Microengineering*, 15(6):1362, 2005.

[7] Metin Renksizbulut and Hamid Niazmand. Laminar flow and heat transfer in the entrance region of trapezoidal channels with constant wall temperature. 2006.

[8] E Galvis, S Yarusevych, and JR Culham. Incompressible laminar developing flow in microchannels. 2012.